

UNIVERSIDAD CARLOS III DE MADRID

ESCUELA POLITÉCNICA SUPERIOR



Tomography of Reactive Flow Jets

September 2015

AUTHOR:

Sergio Redondo Yuste

TUTOR:

Yacine Babou

Contents

1	Introduction	1
1.1	State of the Art & objectives	1
1.2	Introduction	2
2	Method	5
2.1	Tomographic Principle	5
2.2	Tomography Algorithm Implementation	7
2.3	Flowchart	10
3	Method Performance	13
3.1	Parameters Tuning	14
3.2	Relative Size of the distribution	18
3.3	Radial Displacement Effect	19
3.4	Particular Cases	21
3.5	Noise effect	24
3.6	Validity of the Program	26
4	Realistic Application	27
4.1	Temperature Estimation	27
4.2	Application to a Xenon Plasma Jet	31
5	Summary & Conclusions	37
5.1	Future steps	38
	Appendices	39
A	Trigonometric Interpolation	41
B	Budget	43

List of Figures

1.1	Tomography of a brain: American Heart Association Journals	2
1.2	Example of a reconstruction	3
2.1	Initial Distribution	5
2.2	Top View of the Distribution	6
2.3	Tomographic principle ([1])	6
2.4	Reconstruction with just the initial four directions	7
2.5	Reconstruction with all interpolated directions	8
2.6	Initial and reconstructed images	9
2.7	Flowchart of the program	10
2.8	Illustration of all the steps of the flowchart	11
3.1	rmse evolution with total local emission	14
3.2	rmse evolution with K	15
3.3	rmse evolution with the number of interpolations done(j)	16
3.4	4 initial directions vs. 3	17
3.5	rmse evolution with the degree of the polynomial	17
3.6	Focusing: initial image (above) vs reconstructed (below)	18
3.7	Two different cases of rmse evolution with the resolution. In Blue, the diameter of the Jet is 150 pxs, in black, 75 pxs	19
3.8	Displacement: initial image (above) vs reconstructed (below)	19
3.9	Protuberance Rotation: initial image (above) vs reconstructed (below)	21
3.10	RMSE evolution with the location of the protuberance	22
3.11	Left: Real images Right: Reconstruction	23
3.12	Left: Real images Right: Reconstruction	24
3.13	Noise due to unsteadyness on the distribution	25
3.14	Noise due to measurements	25
4.1	The equations above represent the red line	28
4.2	Reconstruction of a simple temperature distribution	29
4.3	Reconstruction of an irregular temperature distribution	30
4.4	Reconstruction of a hollow temperature distribution	31
4.5	Reconstruction of a stretched temperature distribution	32
4.6	Light emitted due to electrons	34
4.7	Reconstruction of the temperature and the density distributions	36

Acknowledgements

To my tutor, Yacine Babou, for his dedication and continuous help even on Sundays.
To my friends, for all kinds of help received. Specially to my university classmates, who made the journey way more easy.
Finally, to my family, for supporting me during so many years, this is also yours. To my dad, Mario, for teaching me what hard work is. To my mum, Rosa, for being there, no matter what. It must be hard dealing with the three of us, thanks for being a Superwoman. Last, and just the opposite to least, to my brother Jaime. Thaks for keep on pushing so hard, you are an inspiration and a teacher for me.

Abstract

The aim of the work developed during this project is to obtain a functional code able of determining local emission distributions on reactive jets just with the intensity profiles recorded by a set of cameras properly located. For this purpose, first of all a good understanding of the tomographic principles must be achieved, in order to understand the benefits and limitations of the method on some possible future experiments of interest in the Aerospace Department. The functional is tested to determine its drawbacks and limitations in experimental situations. In particular, it will be assessed the performance of the method to characterise the temperature inside.

Chapter 1

Introduction

1.1 State of the Art & objectives

Nowadays there is not any technique capable of characterising the internal distribution of some given property of a jet. For this purpose, it is assumed a typical evolution of the flow from the moment when it leaves the exhaust on. Those typical distributions are usually simple, and may give a good approximation when dealing with normal, simple flows.

In the case of reactive jets, its behaviour can be affected by many parameters. Due to this fact, its characterization cannot be based on any assumption. For this reason, tomography techniques are the perfect method for making those characterizations. They do not interfere directly with the media, and they are based in direct measurements of the real flow under study.

The principal objective of this project is to evaluate the performance of a simple tomography method to characterise the distribution of local emission of light. Once this is done, its applicability will be tested by rebuilding the local properties of the flow, such as the temperature or the species density. For achieving this objectives, the following tasks are to be done:

1. Make a stand-alone code able of recreating initial emission distributions with a small error percentage, so that results can be reliable.
2. Determine the functionality of that program, so that limitations are determined in order to take them into account for future experiments.
3. Recreate experimental conditions in order to, with the functional program, determine other properties of the flow.

1.2 Introduction

The concept of tomography is usually related to the medical procedure able to show the internal soft parts of the body in a harmless way. In other words, if asked in the street what a tomography is, Figure 1.1 will appear in almost every single person asked. In fact, that medical procedure is just one of the many applications tomographic procedures have. Many other sciences are including this procedure in the last years, as it represents a fast, relatively cheap and harmless of analysing internal distributions of various medium (gas, liquid, soft matter, porous material).

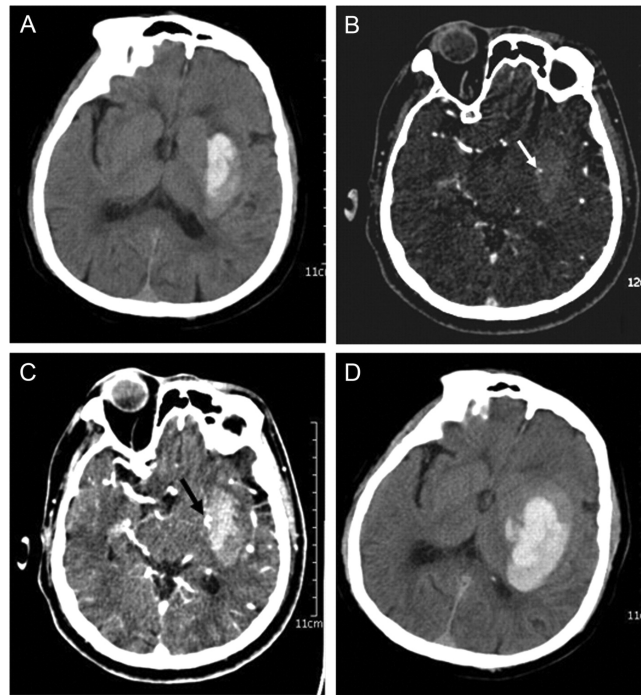


Figure 1.1: Tomography of a brain: American Heart Association Journals

Following this principle, the concept of tomography could be applied to diagnosis of flow jets. In particular, the major advantage of tomography in this field is the fact that it can measure local distributions of various properties without interacting with the medium, assuming there is some magnitude easy to capture at some distance.

Complying with those conditions, during this research investigation the tomographic technique is to be applied to a reactive flow. On a experimental environment, that reactive flow would be that one exhausting an engine. The condition of the jet flow to be reactive is essential, as that way it is assured that the jet emits light. That way, the measurable property would be the light emitted by the jet, easily recordable by means of a camera. In particular, it could be a CCD camera ¹ for instance, in order to achieve proper resolution and quality. Once the intensity is captured by the camera, it can be related to some properties of the flow, and that way, internal measurements of remarkable flow variables could be done.

¹Charge Coupled Device Camera

Throughout this research investigation the method depicted above is going to be tested. The first step will be to create a stand-alone program capable of reconstructing images with acceptable realistic results, as the one shown in Figure 1.2.

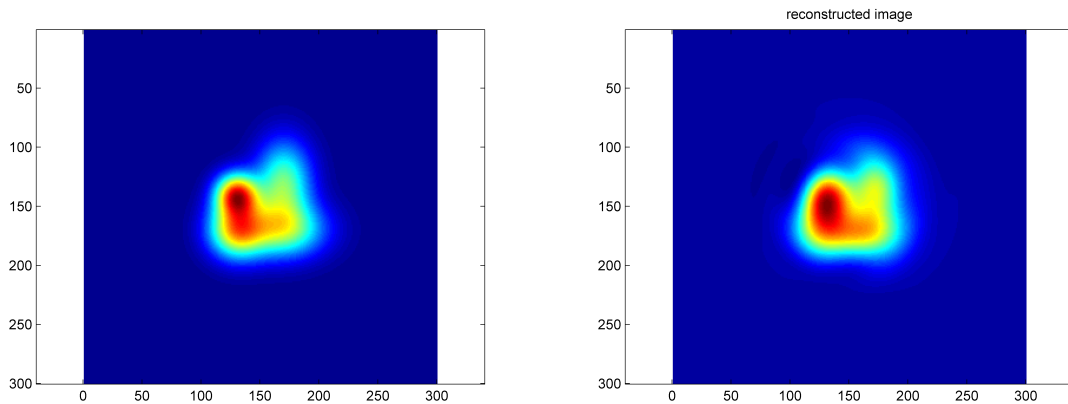


Figure 1.2: Example of a reconstruction

Once this program is working properly, it will be used as a tool for experimental activities of reactive flow jet characterization. As along the project it will not be possible to realise any experiment, the work will focus in relating the intensity captured by the cameras to some other properties that could be useful to know, namely the temperature distribution along the radial direction of the flow.

Finally, some experimental data given by external experiments will be entered and used to achieve a more realistic temperature distribution, checking this way the practical use of the final product.

Chapter 2

Method

2.1 Tomographic Principle

In order to apply tomographic techniques to a jet as explained before, a computer code must be developed. For this purpose, the software Matlab is going to be used, as it has all the features needed.

Consider a jet spreading along the z axis. The technique is to be applied on a chopped section on the x, y plane. From now on, the jet will be left apart, leaving just the chopped section of interest.

A initial distribution of arbitrary shape (Figure 2.1) is created artificially by means of addition of gaussian distributions. All distributions used during this project will be created in the same fashion, by addition or subtraction of gaussian 2D functions on which maximum intensity and x and y deviations are used as control parameters.

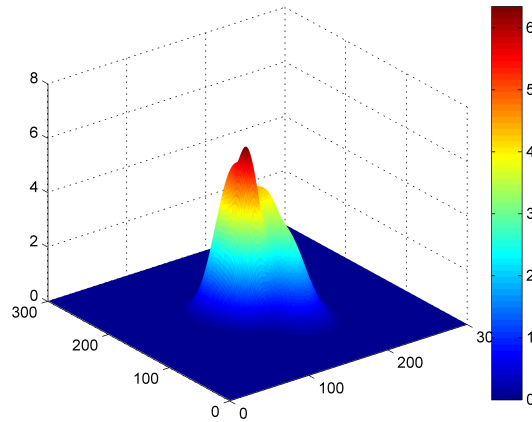


Figure 2.1: Initial Distribution

This distribution just created will work as the local emission distribution $J(x, y)$. The local emission is the quantity of light this gas emits per differential element of volume. It is defined in such a way that the integral of the local emission along any line crossing the centre of the

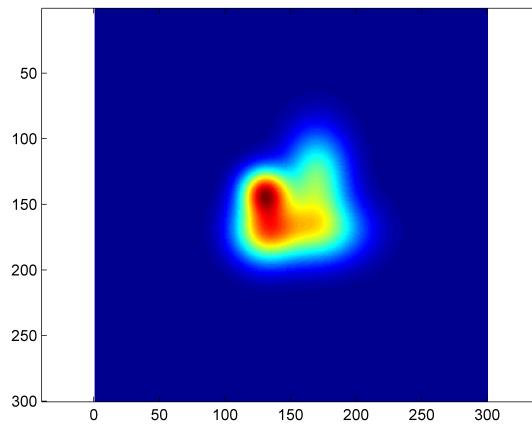


Figure 2.2: Top View of the Distribution

image gives the intensity of the light emitted at a given distance. For a better understanding, refer to Figure 2.3.

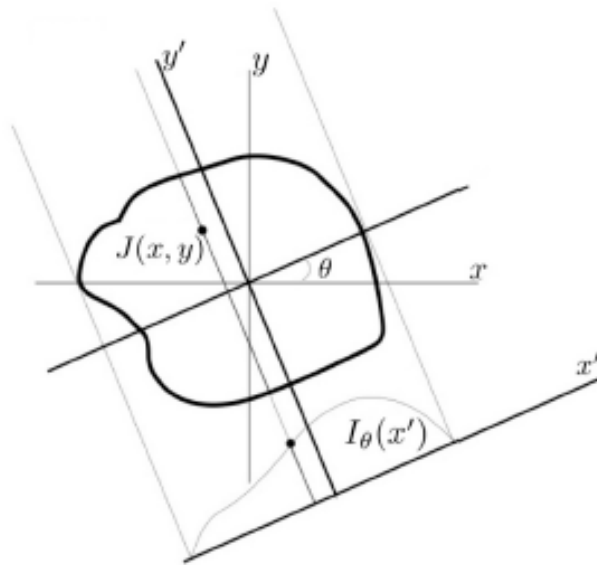


Figure 2.3: Tomographic principle ([1])

The intensity distribution at a given angle θ along the line x' is computed by summation of all differential elements along perpendicular lines to the x' direction.

Tomographic techniques use the Radon transform as the way to relate these intensity distributions with the local emission planar distributions. As Matlab provides a numerical method for the computation of this transform and its inverse by only entering the local emission distribution (or the intensity profiles for the inverse Radon) and the angles for which the intensity is to be or has been computed, any further information about the Radon procedure is going to be provided, as it will be out of scope. Please refer to [2] for more information.

Thus, the only parameter needed to implement this Radon transform function in Matlab are the angles for which the intensity should be computed. Obviously, the greater the number of angles, the better the resulting reconstruction. Unfortunately, in experimental situations, this parameter is strongly limited by the physical means available. Each new angle means another camera needed to record the intensity distribution in that direction. In a first approach, the number of angles will be limited to 4. By assuming that the medium of interest is optically thin, it can be assumed that the intensity distribution in one direction remains constant, regardless of the location from which it is recorded; this means: $I_n(\theta_k) = I_n(\theta_k + \pi)$ with the elements along x' mutually flipped.

Hence, the domain is reduced from $0 - 360^\circ$ to $0 - 180^\circ$. Then, by direct application of Formula 2.1 with $K=4$, the resulting angles for this particular case would be: 0° , 45° , 90° and 135° .

$$\theta_k = 180 \frac{k-1}{K}, k = 1, 2, \dots, K \quad (2.1)$$

Bear in mind that the angles appear in degrees due to the fact that the Matlab radon function requires it.

2.2 Tomography Algorithm Implementation

Once everything needed is available, radon transform can be applied to Figure 2.2, resulting in the left side of Figure 2.4. Four different Intensity distributions can be seen there, each one corresponding to one k direction. When the process is done backwards, that is, when the inverse radon is used for reconstructing the initial local emission distribution, the right hand-side of Figure 2.4 results. By comparing with the initial figure, this is obviously a really poor result, but with just 4 directions is the best one that can be achieved.

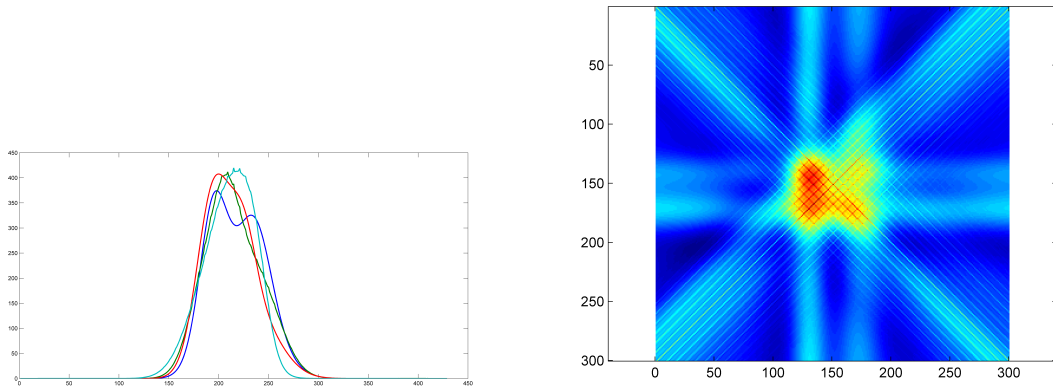


Figure 2.4: Reconstruction with just the initial four directions

There is an important fact in this step of the process, which is that the intensity distributions just mentioned will be the real input in an experimental case. They are then the raw material for the reconstruction, and hence, the best place to implement improvements in order to achieve much better results. The problem comes from the low number of directions available. As it cannot be increased directly, an interpolation can be done, in order to increase the number of directions artificially. Certainly, some resolution might be lost within the process, but this is still the best possible solution. Taking the procedure from [3], a trigonometric interpolation has been implemented in the program. Refer to Annex A to see the procedure.

For the interpolation to take place, the intensity profiles must be written in polynomial form. $c_n(\theta_k)$ are the n coefficients of the polynomial that defines the intensity distribution of the k direction. Hence, with the implementation of this procedure, any $c_n(\theta)$ can be computed, regardless of the θ desired. Note how for using this, the intensity distributions must be written as polynomials. The degree of these polynomials chosen will affect the result, and it will vary depending on the complexity of the shape. The coefficients $c_n(\theta)$ are such that:

$$I(x', \theta_k) = \sum_{n=0}^N c_n(\theta_k) x'^n \quad (2.2)$$

Once this procedure is applied to the initial set of Intensity distributions, a new set is created. On the left hand-side of Figure 2.5 it can be seen this new set when the procedure has been applied 4 times. This, with $j=4$ times the procedure, and initial $K=4$, results in a total of $L = 2^j K = 2^4 4 = 64$ directions.

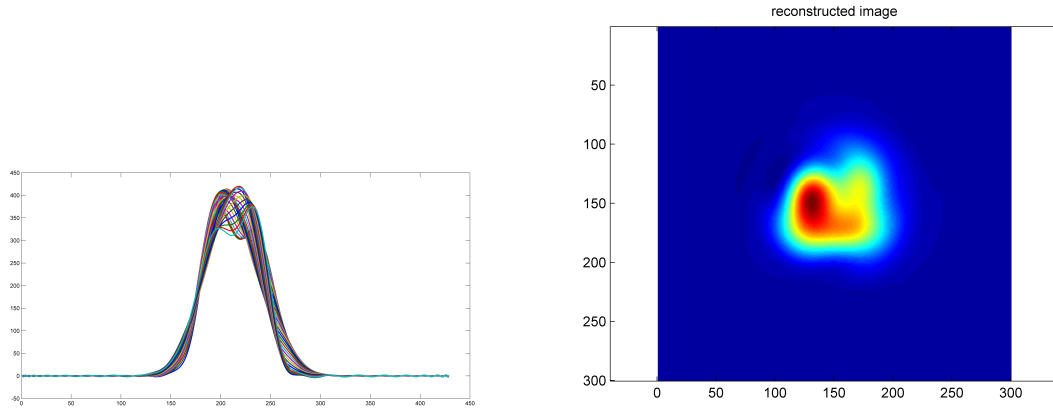


Figure 2.5: Reconstruction with all interpolated directions

With the new set of Intensity distributions, the reconstruction process results in a much better result than before; it can be seen in the right hand-side of Figure 2.5

For a better understanding on how the result has improved, it can be used the Root Mean Square Error (RMSE):

$$RMSE = \sqrt{\frac{\sum_{i=1}^x \sum_{j=1}^y (J^{rec}(i, j) - J(i, j))^2}{N}} \quad (2.3)$$

The relative RMSE is going to be used during the report as the way of finding the optimal results. It is important to remark that it is not absolute but relative, so that it just works by comparing values of different cases, being this way easy to determine what is better for our purpose. In this particular case, The RMSE before the trigonometric interpolation was 0.534, and now, after it, is 0.058, that is, one order of magnitude smaller than before. The final comparison between the initial and the reconstructed distributions can be seen in Figure 2.6.

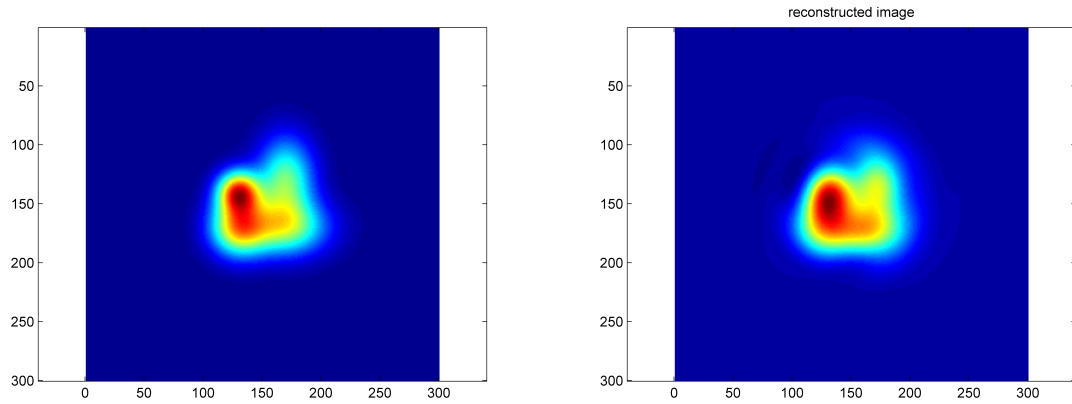


Figure 2.6: Initial and reconstructed images

2.3 Flowchart

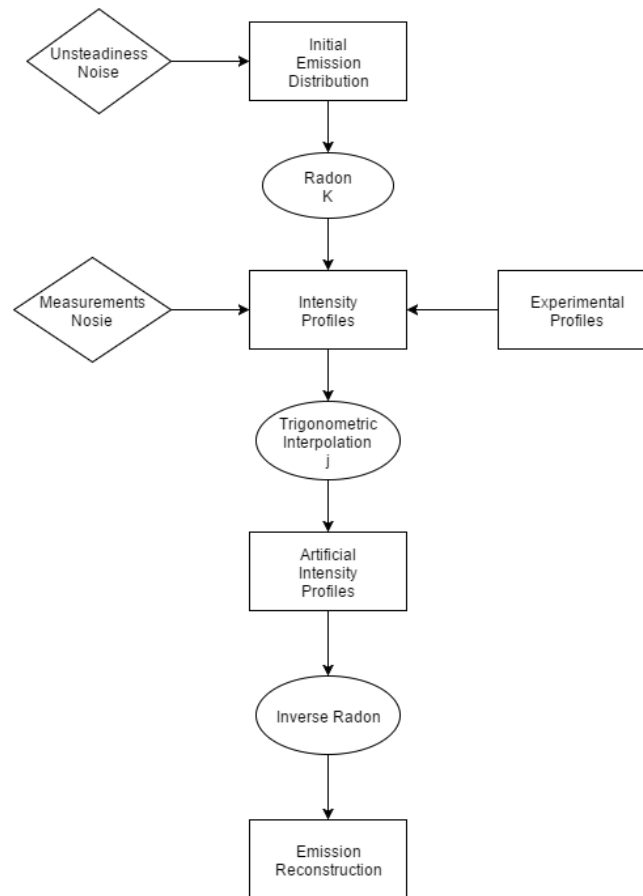


Figure 2.7: Flowchart of the program

Figure 2.7 shows in a simple way the algorithm developed for the program, whose parts were explained in the previous sections. It gives the opportunity of starting with an initial, theoretical emission distribution or if the work is done experimentally, with some real intensity profiles. For the theoretical case, it exists the possibility of introducing noise as a way of recreating experimental conditions.

In Figure 2.8 it can be seen all the steps formulated in the Flowchart analysed for a hollow theoretical distribution without noise applied. The effect of the noise, together with that of the most important parameters appearing in the flowchart will be studied in the next chapter.

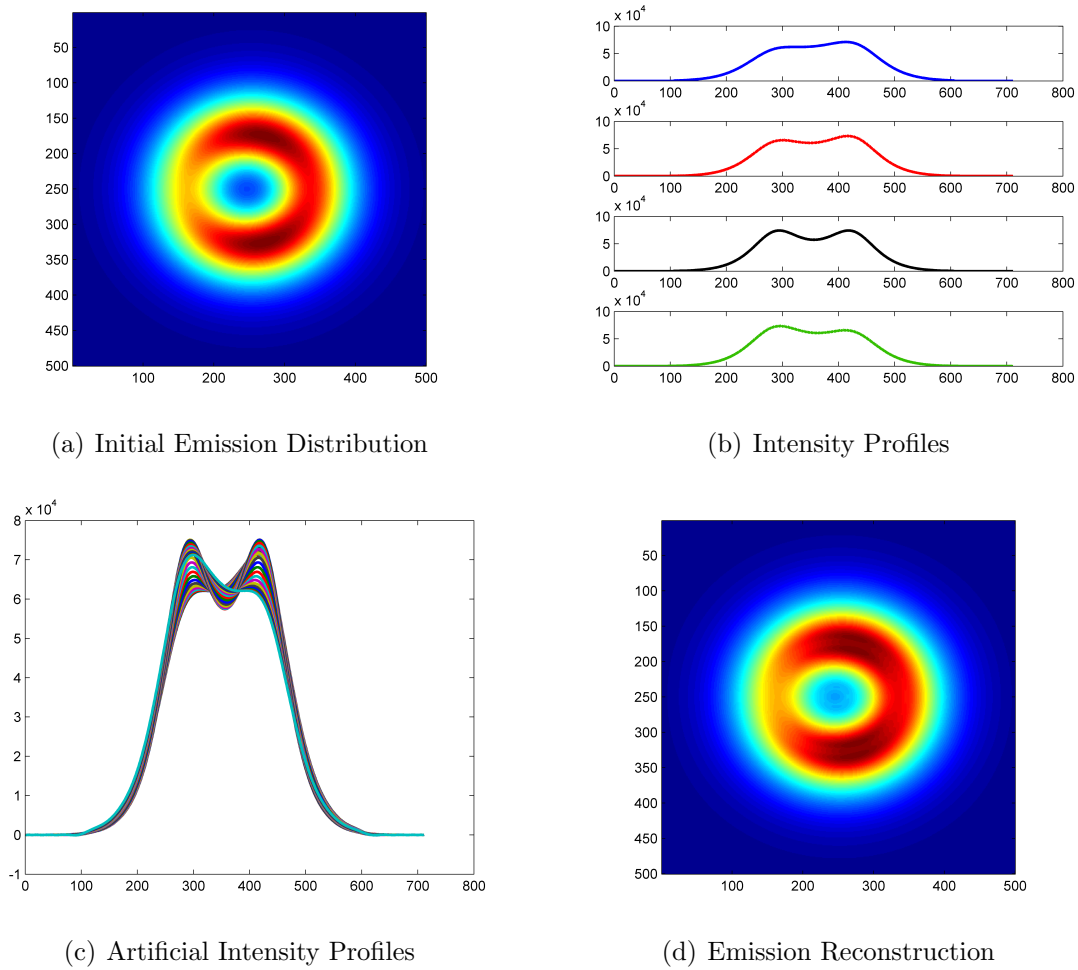


Figure 2.8: Illustration of all the steps of the flowchart

Chapter 3

Method Performance

Once it has been demonstrated that the code in charge of performing the tomography is functional and the results are acceptable, there are a set of features regarding future applications that should be checked. Some of the parameters appearing along the development of the program are really important, as they are the ones that actually define the performance of the code. These parameters are going to be tuned in the next section, together with some other features.

For this purpose, the RMSE is going to be used. Different cases will be compared until the lowest possible value of the RMSE is found. The case corresponding to this lowest possible value will determine the optimal value of the parameter under study.

3.1 Parameters Tuning

Before getting into matter, it is important to understand how does the RMSE evolves with the values it is facing. In Figure 3.1 it can be seen how a linear behaviour relates the RMSE and the intensity of a simple gaussian distribution. As might be expected, the greater the values the tomography is dealing with, the greater the difference between the initial and the final distributions. It should be remarked that this fact does not mean that the quality is worse, as the tendency is to increase linearly.

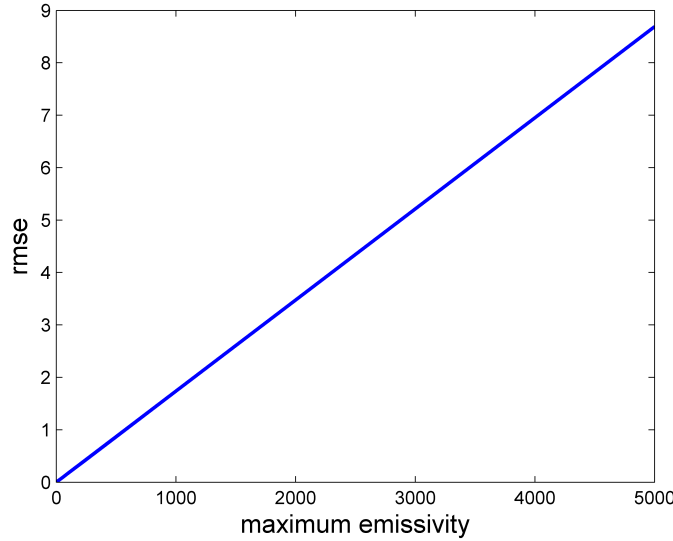


Figure 3.1: rmse evolution with total local emission

The most important parameters that should be tuned are:

- **K**, the number of initial recording directions, or in other words, the number of divisions in 180° that determine the directions in which the intensity distribution is computed for the radon transform.
- **j**, the number of times that the trigonometric interpolation is done. This determines the final number of directions(L) for which artificial Intensity distributions are determined ($L = 2^j K$). Is the input to the inverse radon procedure, that remakes the local emission distribution.
- **polynomial degree**, This parameter will not remain exactly constant, as opposed to the other parameters. Depending on the complexity of the Intensity distributions, it will vary in some extent. It is important as the trigonometric interpolation is done for these coefficients.

The first parameter evolution can be seen in Figure 3.2. The distribution used for this case was a simple centered gaussian distribution. Obviously, the greater the number of directions used, the better the result in terms of RMSE. It is interesting to see that just with 8 directions is enough to achieve what is the lowest possible value (0.0073), as from that value on the RMSE remains constant.

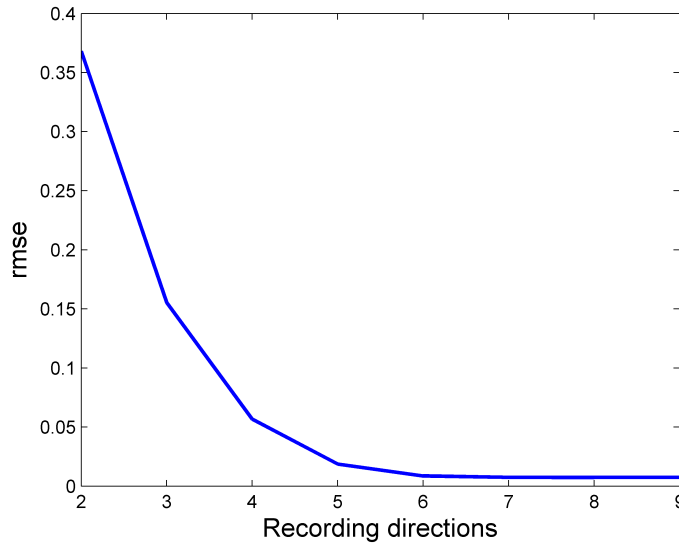


Figure 3.2: rmse evolution with K

Unfortunately, the conclusions extracted from this Figure are not useful, as the fact that $K_{ideal} = 8$ is limited by the physical means. 8 cameras recording is already a great economic investment. In any case, if one has the possibility, that investment could be done in order to achieve better results.

The second parameter, j has any limitation, so the results will be really determining for the tuning. It is important to determine that these 2 parameters, j and K are of great importance due to the fact that they are the 2 contributors to the final number of Intensity profiles used as input, L , through the formula aforementioned $L = 2^j K$.

It can be seen a huge improvement in the initial rounds, while after the second interpolation done the resulting distribution does not improve greatly. The minimum value achievable appears for the first time for $j = 3$. Thus, from now on, this parameter will remain untouched in this value.

Once j is closed, it is time to go back to the K tuning. As the proper value was not worth to use, j can be used to determine an acceptable value for L , that will result in a lower (acceptable) value of K with the same performance as if K was 8. As K and L are the same in figure 3.2, let's set $L = 8$, then $L = 2^j K; 8 = 2^3 K$; resulting in $K = 1$. $K=1$ is not an acceptable value, as any interpolation can be done. For an interpolation to take place, K must be at least 3.

As the behaviour of the tomographic technique can be really good understood through visual inspection, a test was done, whose results can be seen in Figure 3.4. For a random distribution, several K values were tested, concluding that the proper value was between 3 and 4. Finally, as still some difference can be appreciated from $K = 3$ to $K = 4$, the K parameter was tuned to be always equal to 4.

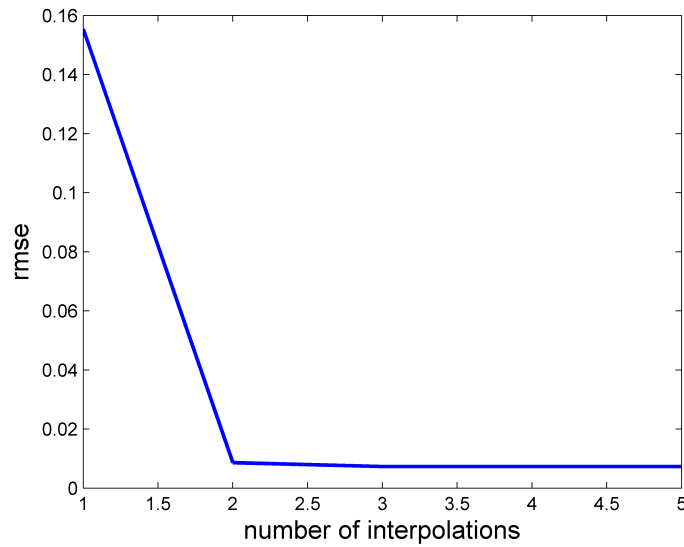


Figure 3.3: rmse evolution with the number of interpolations done(j)

Finally, the last parameter remaining is the degree of the polynomial. As said before, this one will not remain exactly constant, as it depends on the complexity of the shape under study. Thus, the RMSE evolution will be done for 2 different distributions, a simple gaussian and a more complex one. Results can be seen in Figure 3.5.

The simple case, corresponding to the blue line, achieves the lower values of RMSE for polynomial degrees close to 30. On the other hand, the complex distribution RMSE (black), keeps descending until the degree is close to 40. With any further investigation, the degree will be set to some value between 30 and 40, tuning it whenever due to the shape introduced for analysis this value can result of some importance.

Finally, the parameters are:

K	4
j	3
polynomial degree	30 – 40

Table 3.1: Final parameters

Once these parameters are well tuned, it is time to start with a deeper analysis of the code. In order to use the tomography for future experiments, it should be checked whether if some limitations apply to it. In the next pages some interesting shapes together with some other parameter will be analysed, always in the context of a reactive jet analysis. This way, the real opportunities that the program provides will be well understood, and its validity will be measured through its functionality.

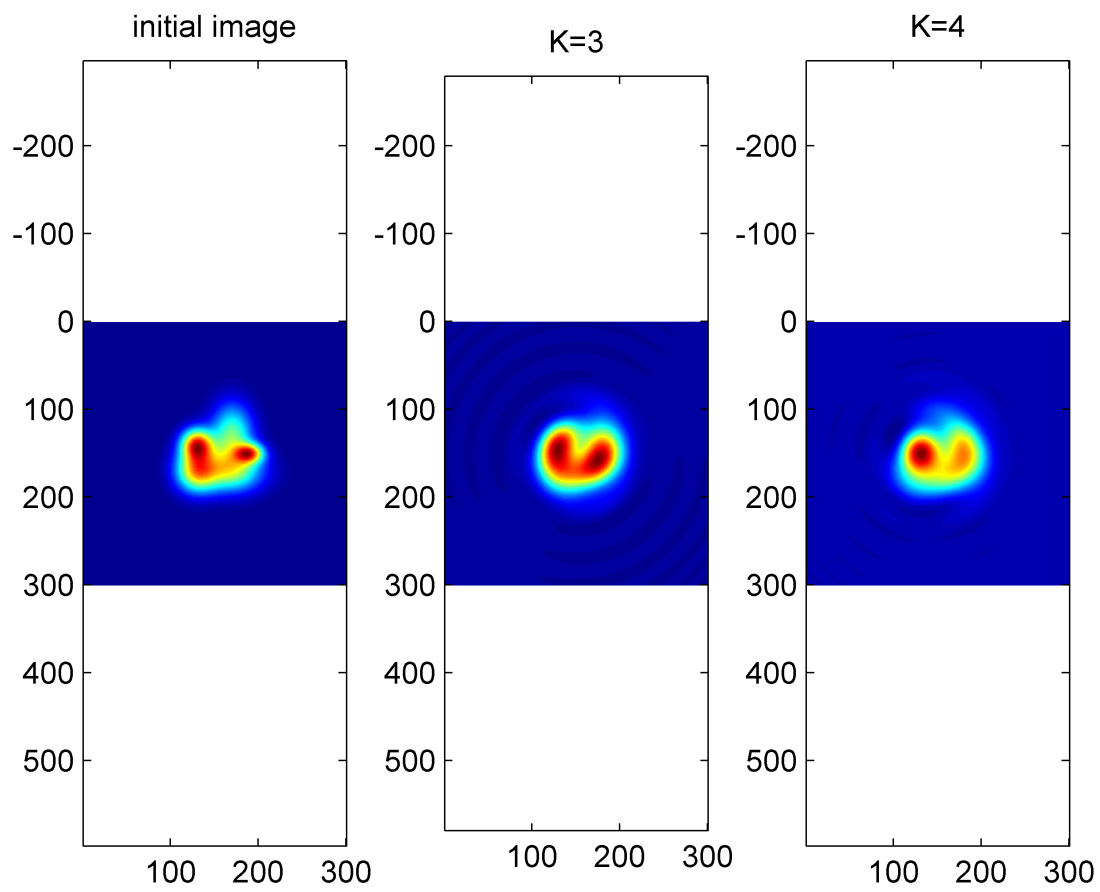


Figure 3.4: 4 initial directions vs. 3

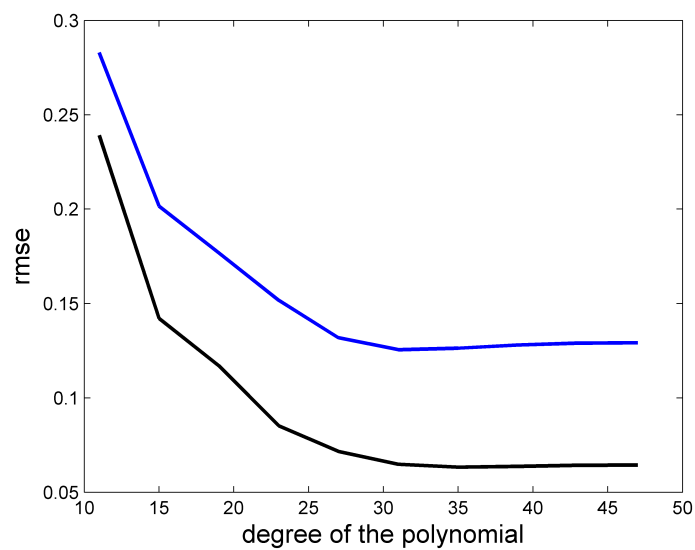


Figure 3.5: rmse evolution with the degree of the polynomial

3.2 Relative Size of the distribution

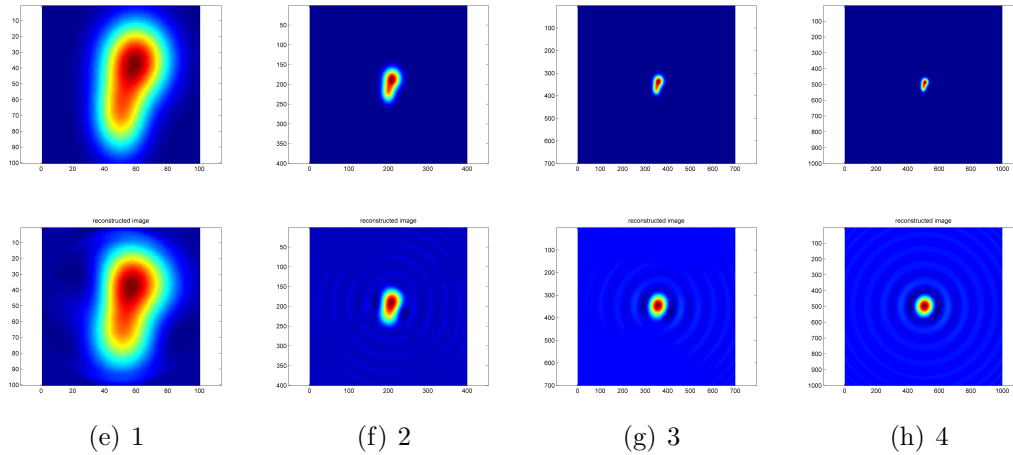


Figure 3.6: Focusing: initial image (above) vs reconstructed (below)

Focusing the image recorded properly within the limits of sight can be really determining. In the program created, the focusing capability is defined through the length of the line x' , related with the Intensity distribution. Usually having great resolution is really useful in terms of being able of capturing every single detail of the distribution. On the other hand, when working with bad focusing techniques the image can get somewhat lost in the middle of the picture, so that the effect achieved counteracting the good resolution; the quantity of pixels containing important information is really low compared with the total number of pixels, making a bad reconstruction out of a initial good resolution environment.

What was explained in the last paragraph is illustrated in Figure 3.6. There it can be seen the evolution of a distribution (initial and reconstruction) when the relative size of the distribution with respect to the total area decreases, letting the distribution to get lost in the middle of the image. As it can be seen, at the beginning the result is the expected one. There is a point where the surroundings of the jet acquire a wavy behaviour (step 2). This is the critical point, as when those waves start to disappear, the quality of the jet reconstruction is lost completely, and from the initial oval shaped distribution, in cases 3 and 4, the reconstruction results in a circle.

The best results are achieved, by inspection of Figure 3.7, when the diameter of the jet fits within the 25-30% of the lateral length. This can be concluded after checking that the lowest possible RMSE is achieved, for both cases shown and all the ones analysed, when the lateral profile is four times the diameter. As the distributions are not circular, the diameter is taken as the greatest length between opposite points provided that their intensity is a 40% of the maximum one.

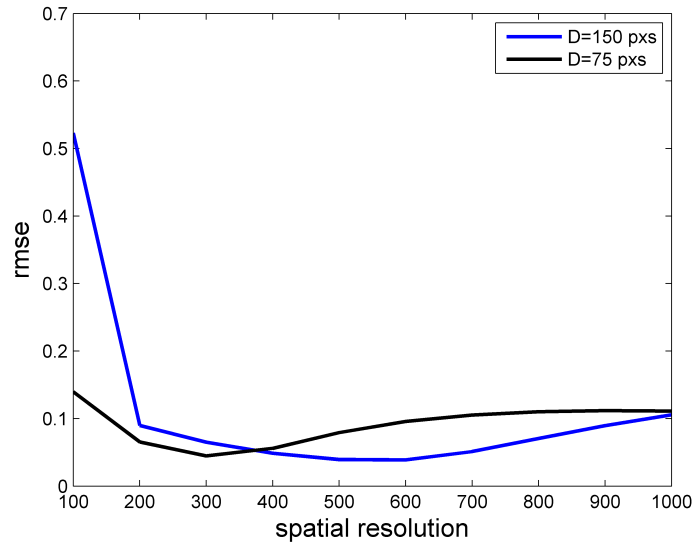


Figure 3.7: Two different cases of rmse evolution with the resolution. In Blue, the diameter of the Jet is 150 pxs, in black, 75 pxs

3.3 Radial Displacement Effect

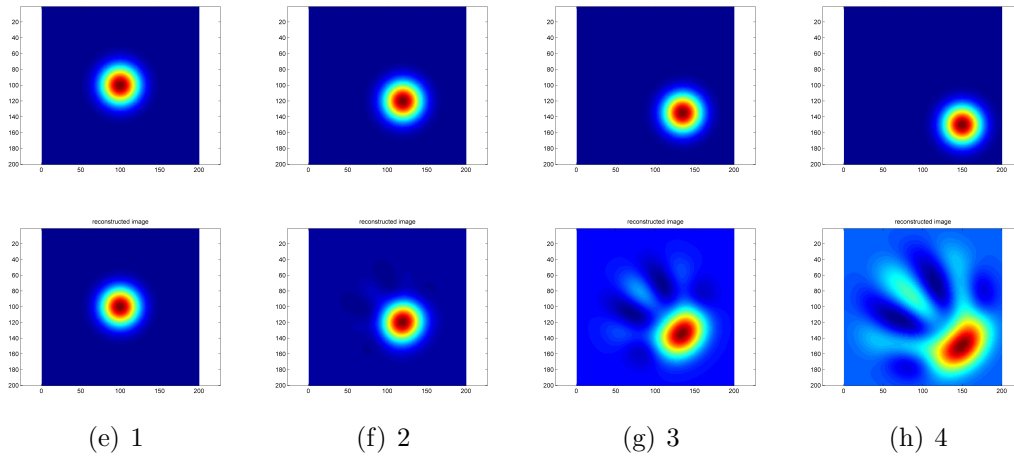


Figure 3.8: Displacement: initial image (above) vs reconstructed (below)

Another interesting fact when recording a jet could be how important is to keep it in the middle of the image. As Radon transform works by assuming radial properties, the displacement of the distribution from the central point might cause the reconstruction to be really poor in terms of quality. Here it will be established to which extent a departure from the central position is acceptable or not.

In order to analyse this, a simple gaussian distribution is forced to be moved from the central point of the mesh (100, 100) to the point (150, 150) in 10 steps. The result can be seen in Figure 3.8. Only some steps of the evolution are shown for the sake of simplicity. It can be seen how

the initial results are good (as expected, the initial and reconstructed images look the same). Already in step 2 some stains are appreciated on the closest part of the distribution to the center of the mesh. Those stains get greater while the evolution goes on, and the reconstruction of the jet is already in step 3 quite affected, leaving the initial circular shape to look like an oval instead.

Hence, it can be concluded that up to the 5th step (corresponding to a mid-state of images 2 and 3) the reconstruction is acceptable. This step corresponds to a displacement of 35 pixels (radial displacement). This compared to the 200 pixels of resolution, represents the 17.5% of the resolution. Thus, the center of the jet must be contained, if possible, within a circle of radius equal to 17.5% of the lateral resolution.

3.4 Particular Cases

After having completed some initial analysis on the functionality of the program varying some remarkable parameters, it is time to analyse some specific cases. In the end, the program is intended to be able to work with jets. Thus, some particular features that might appear within a jet are of great interest and must be tested. Although these might be many, here three cases will be studied: A circular jet with a lateral protuberance, varying the location of it, distributions with two peaks of intensity instead of just 1, and finally, some hollow distributions.

Due to the turbulent regime that flows exhibit when exiting an exhaust, gases might diverge from the theoretical column they would be following in other case. This divergence might occur just on one side, making the jet completely asymmetric by creating what would look like a lateral protuberance from a top view.

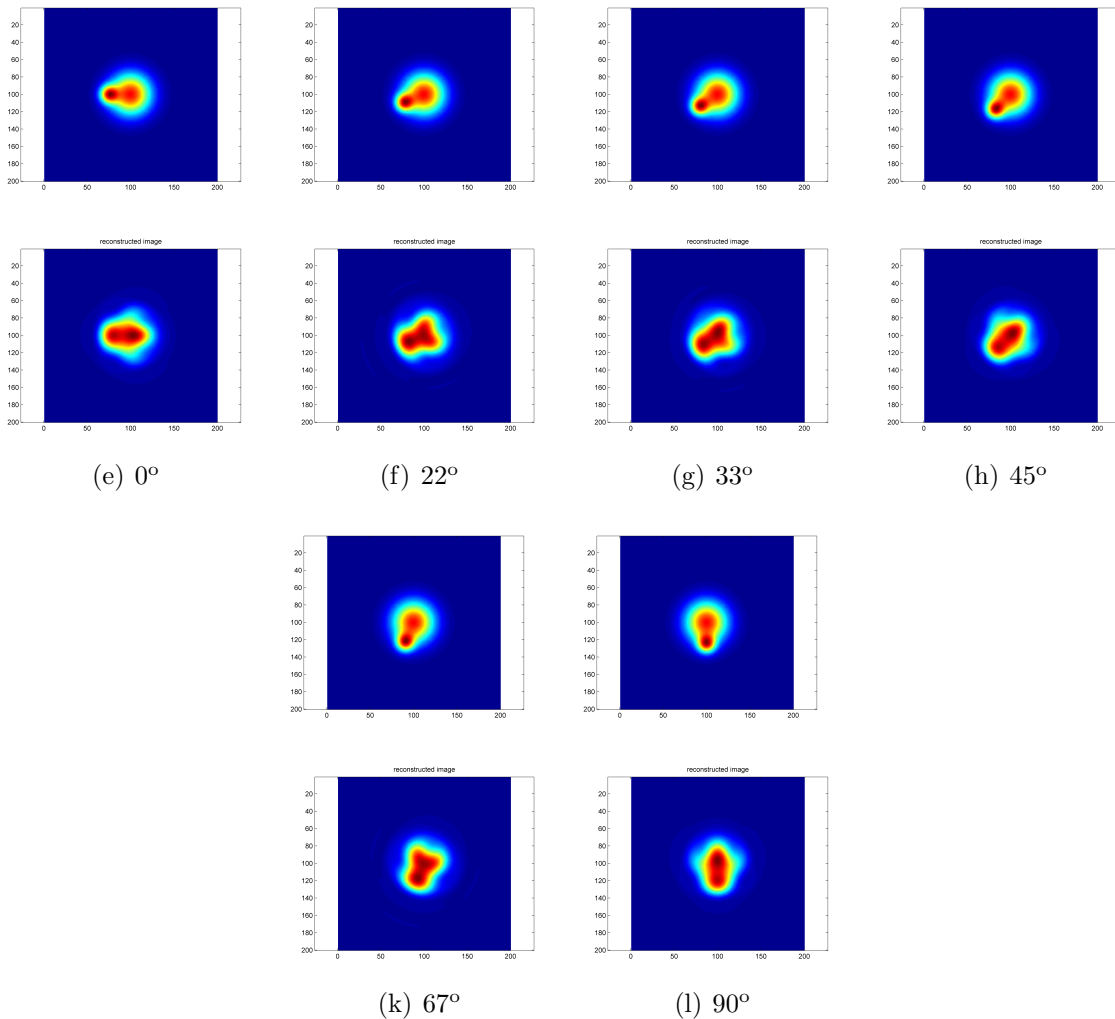


Figure 3.9: Protuberance Rotation: initial image (above) vs reconstructed (below)

As for the tomography just 4 precise locations are being recorded, the location of these

protuberances might be significant. Recall that the angles used in our case are $0^\circ, 45^\circ, 90^\circ$ and 135° . In Figure 3.9 it can be seen how the reconstructions of some distributions look like, depending on the position of the protuberance.

Taking into account the angles chosen, the figures can be divided in three groups: Those pointing to an original direction ($0^\circ, 45^\circ$ and 90°), those corresponding to first order interpolations (22.5° and 67.5°) and a last one corresponding to a second order interpolation.

It can be seen on a first inspection that even the images with protuberances pointing to original directions do not achieve realistic reconstructions. In any case, the result might be considered acceptable. On the other hand, when the protuberance does not point to an original direction, the result diverges greatly from the original image. The fact that it point to a first order or second order location does not seem to affect on a great amount, as in both cases the result is just bad.

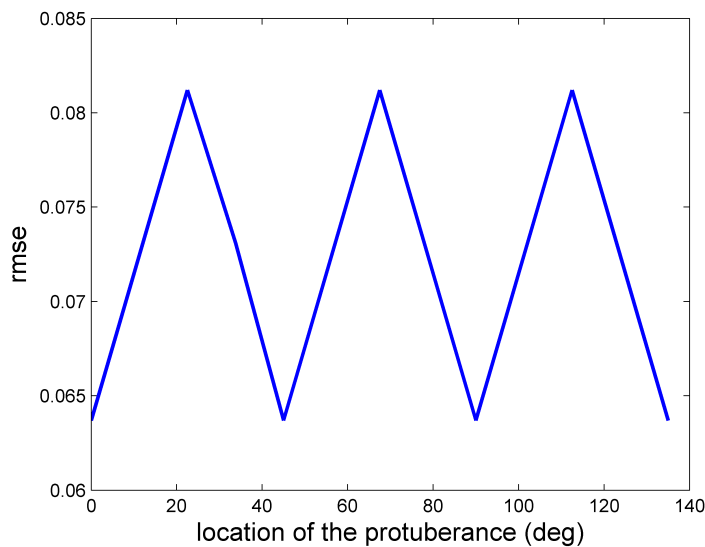


Figure 3.10: RMSE evolution with the location of the protuberance

To understand better what is happening, the RMSE values were captured for all the cases, and in figure 3.10 it can be seen the result. The lowest values of RMSE are achieved when the protuberance is located in original directions, whereas the worst result coincides with the locations of first order interpolation. This is due to the fact that these locations are the ones located further from any original direction, making the resulting interpolation a bad approach.

It is really interesting to see how from those maximum and minimum points, the RMSE follows a linear relation. This was checked by computing extra RMSE values for angles in the middle of this zone.

The second particular case studied is the appearance of more than one peak within the jet planar distribution. Again, based on the fact that the turbulent regime is, in principle, really difficult to foreseen, a possible scenario would be the division of the tip of the jet. This is the case recreated in the following images, with its corresponding results.

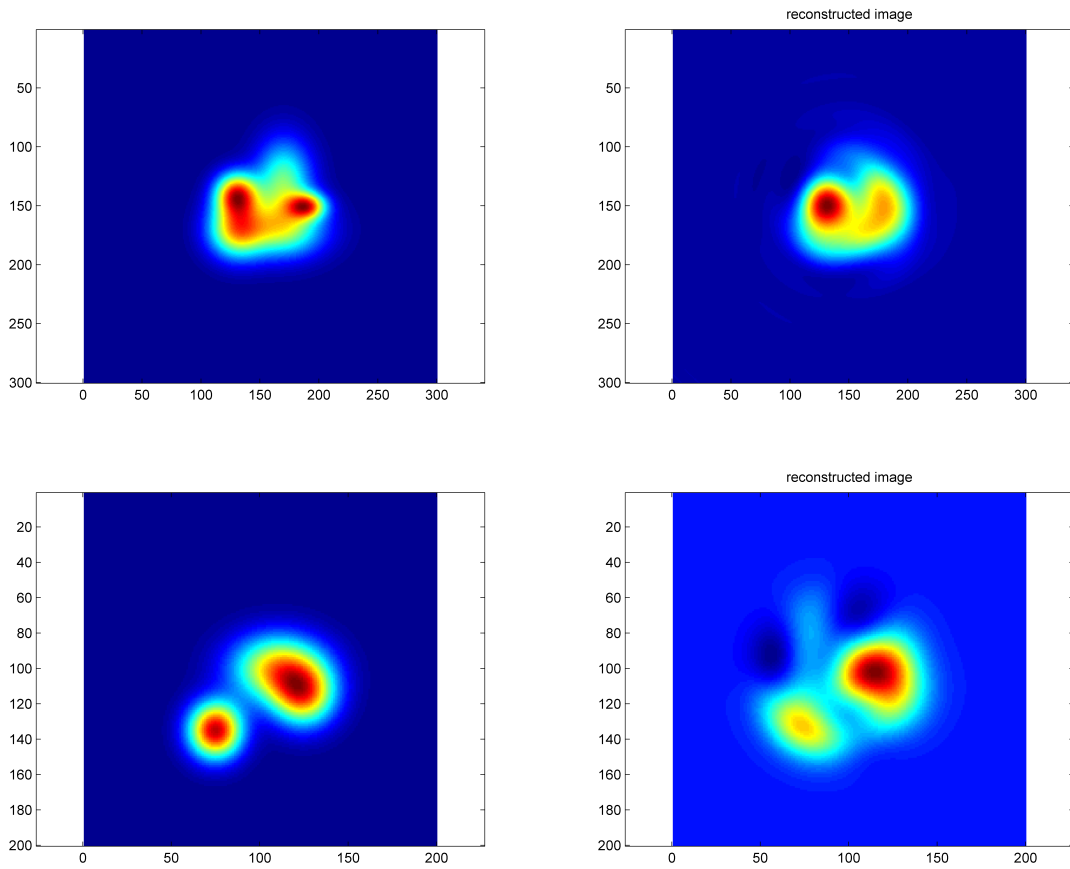


Figure 3.11: Left: Real images Right: Reconstruction

Two different distributions appear in Figure 3.11, one with the two peaks still close to each other and another one with a greater separation. In both cases it can be seen by direct inspection that the result of the reconstruction is not realistic. To throw some numbers to it, the RMSE values are 0.16 for the case where the jets are well separated and 0.22 for the case where the jets are closer to each other.

It is interesting to see how the lower value is achieved for the case that could seem more complex on a first instance. This is due to the fact that two peaks close to each other would require a really precise polynomial fitting that is really difficult to achieve.

Another case, simpler than the other two studied and really easy to find is a hollow distribution. There are a considerable number of engines whose exhaust nozzles present an annular shape. Due to this fact, the initial shape of the distribution just after leaving the nozzle will be a ring with a quasi spherical shape.

Thus, it is critical to check whether if the program is prepared to recreate such a situation, as it might be quite common. The hollow distributions studied can be seen if Figure 3.12.

As it can be seen, the reconstructions seem to fit in a good manner the initial distributions.

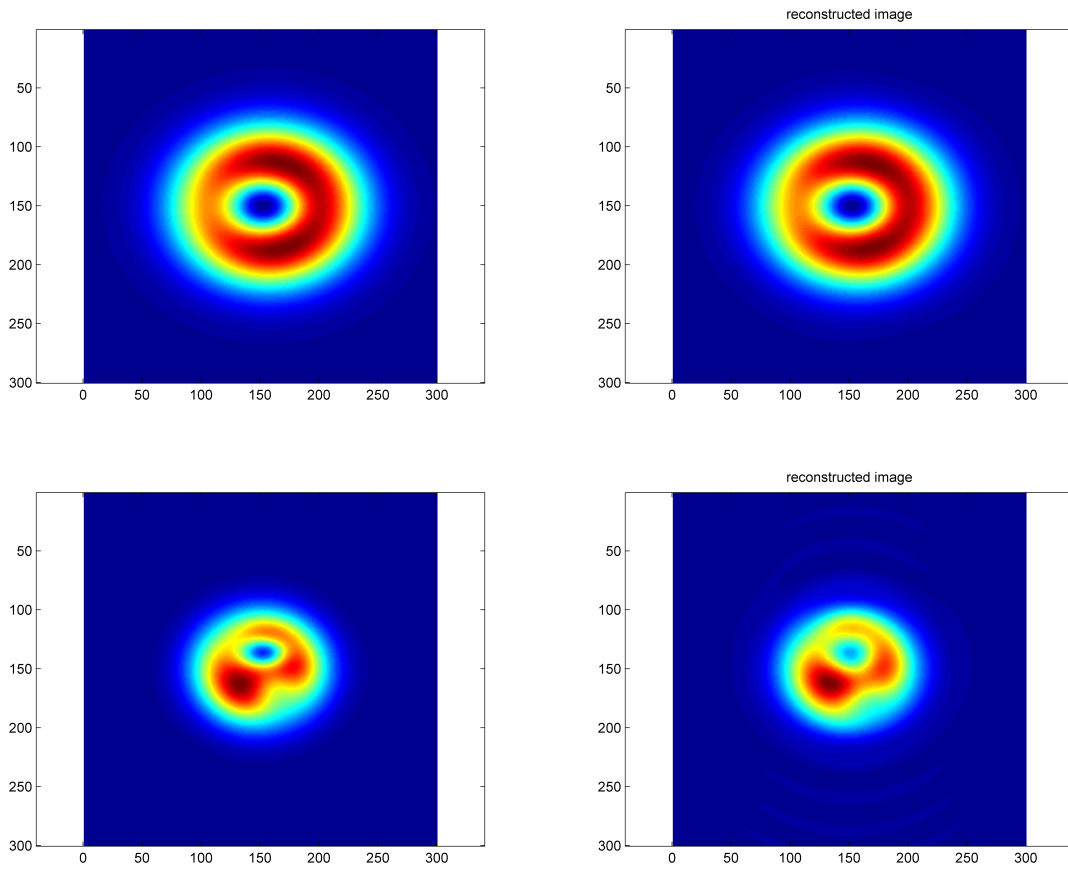


Figure 3.12: Left: Real images Right: Reconstruction

The first case represents a greater distribution, which implies a greater hole in the middle. Thanks to this fact, the reconstruction fits almost to perfection the real image, achieving an error of the local emission in the middle of the image of the 8%.

On the other hand, the second case presents a more irregular shape, the distribution is smaller, and the hole left by the annular exhaust is smaller. This distribution would correspond to a latter point in the timeline, where the recording point is somewhat further from the exhaust. This time, the reconstruction in the middle is not that good. The error of the local emission in the midpoint of the grid is of the order of the 18%. This is related with what was explained in the case of the double peaked distributions, of having a bad polynomial fitting due to the closeness of various peaks.

3.5 Noise effect

Due to possible future experimental procedures where the program might be embedded, the performance of it in a noisy environment should be studied and checked whether if under these circumstances, the results are still reliable. There are two principle sources of noise, as depicted in the flowchart in 3.3.

The first source of noise is due to the unsteadiness of the distribution. This noise depends on the control that can be exerted on the experiment. If the conditions of the jet and its environment can be easily controlled, this noise could be wiped out or reduced to a minimum value. In other case, it should be taken into account. In Figure 3.13 it is shown its effect on a distribution.

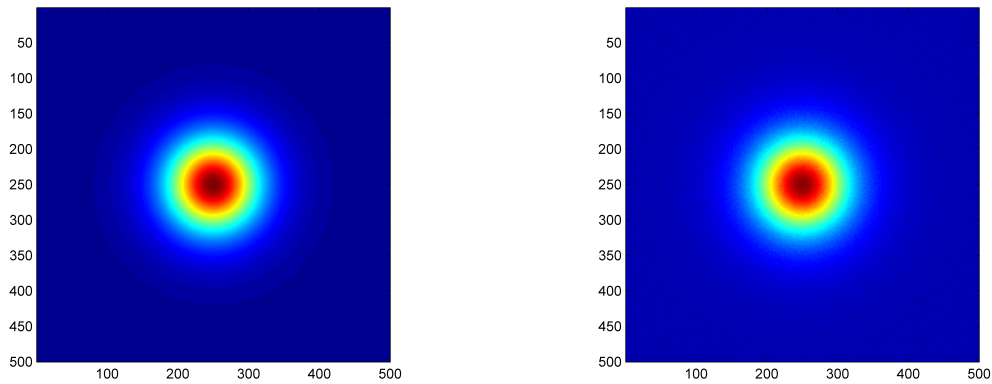


Figure 3.13: Noise due to unsteadiness on the distribution

The other source of noise is the one inherent to the measurement devices used to capture the intensity profiles. This sound enters in the original captured profiles. It should not be wiped out in any case, as in every experiment it is always present. In any case, the intensity of it can be reduced as a function of the precision instruments used. Its effect can be seen in Figure 3.14.

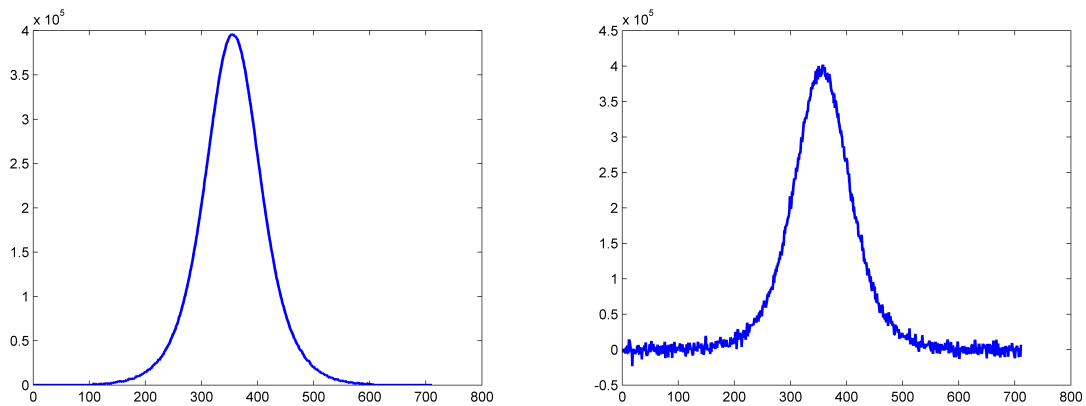


Figure 3.14: Noise due to measurements

3.6 Validity of the Program

After having checked the most meaningful parameters affecting the quality of the reconstruction, the following conclusions can be extracted:

- The center point of the distribution should be contained within an area of a radius of the 25-30% of the lateral profile, as further displacements provoke great distortions of the shape.
- The diameter of the distribution should not be smaller than a 20% of the lateral length, in order to make the program able of capturing all the details of the distribution.
- The distribution should be single-peaked, meaning that it should not have more than just one local maximum which would correspond to the absolute one.

It can be assured that provided a distribution or lateral intensity profile which fulfils these constraints, the reconstruction obtained out of it will be valid to extract information and conclusions out of it.

Chapter 4

Realistic Application

Once it has been demonstrated to be possible to obtain a reliable local emission distribution, it is time to relate these data with some other physical properties that can be useful from a research point of view. Obtaining those distributions would be relevant as due to the great temperatures usually faced in this kind of experiments or situations, measuring them directly is usually difficult and approximations are used based on other easier measurements.

4.1 Temperature Estimation

Lets consider now a jet of air plasma at 1 atmosphere and high temperature. It is then possible to relate the emission directly to the temperature of the flow:

$$J = A10^{TB} \quad (4.1)$$

and inversly:

$$T = \frac{\log_{10} \frac{J}{A}}{B} \quad (4.2)$$

Equations 5.1 and 5.2 show the relation between the temperature and the local emission. This relation is obtained by means of theoretical calculations of the local radiative emission of air plasma in the range of temperatures between 2000 and 15000 K, leading to the graph shown in Figure 4.1. For the sake of simplicity, when working in a known range of temperatures it can be established an linear equation to represent a fraction of the line.

In the case under study, the temperatures will be introduced theoretically. Thus, they can be totally controlled. For this purpose, the equation of the red-dashed line can be used. Thus, the parameters A and B that define a line in a logarithmic-logarithmic chart, can be computed from that line.

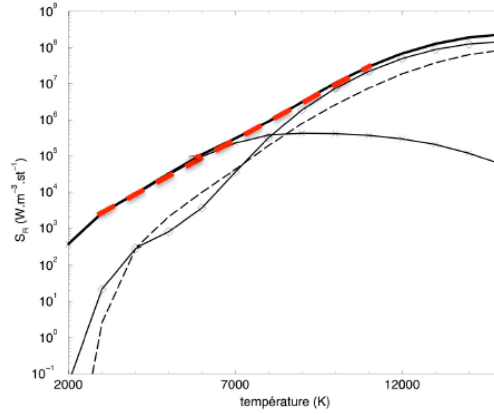


Figure 4.1: The equations above represent the red line

Once those relations are established, it is just a matter of introducing them in the previous code in order to have a temperature reconstruction. Four different cases are to be studied, to ensure proper performance:

<i>Case</i>	<i>Distribution</i>	$T_{central}$
1	<i>Reference</i>	15000
2	<i>Irregular</i>	12000K
3	<i>Hollow</i>	1200
4	<i>Stretched</i>	1000

Table 4.1: Cases under study

In Figures 4.2, 4.3, 4.4 and 4.5 the reconstruction of different temperature distributions are shown. It is important to recreate on a first instance the simple distribution, as the RMSE value can be used that way by comparing it to this simple case. The RMSE value obtained for that simple case is 11.99. Just by inspection it can be seen that the case shown in Figure 4.3 did not achieve a realistic reconstruction, as the shape obtained is quite different from the initial one. A RMSE in this case of 33.56, almost three times the one of the simple case, illustrates pretty well this fact.

In any case, as the temperature is the object of study, the analysis can go one step further. Interesting applications of this method include the possibility of obtaining the internal temperature of the distribution. It can be seen that the location of the maximum value in both cases is practically the same (with less than 5% error). The error of that maximum obtained from the reconstruction is 1%, meaning that although the shape obtained is not the proper one.

In the case of the hollow distribution, shown in Figure 4.4 the reconstruction seems to have achieved the desired results. In fact, the RMSE shows that the quality is close to the one of the irregular case, as it is again 3 times greater than the value obtained for the simple case. The lack of coincidence with the original figure that lies behind this bad RMSE result is the

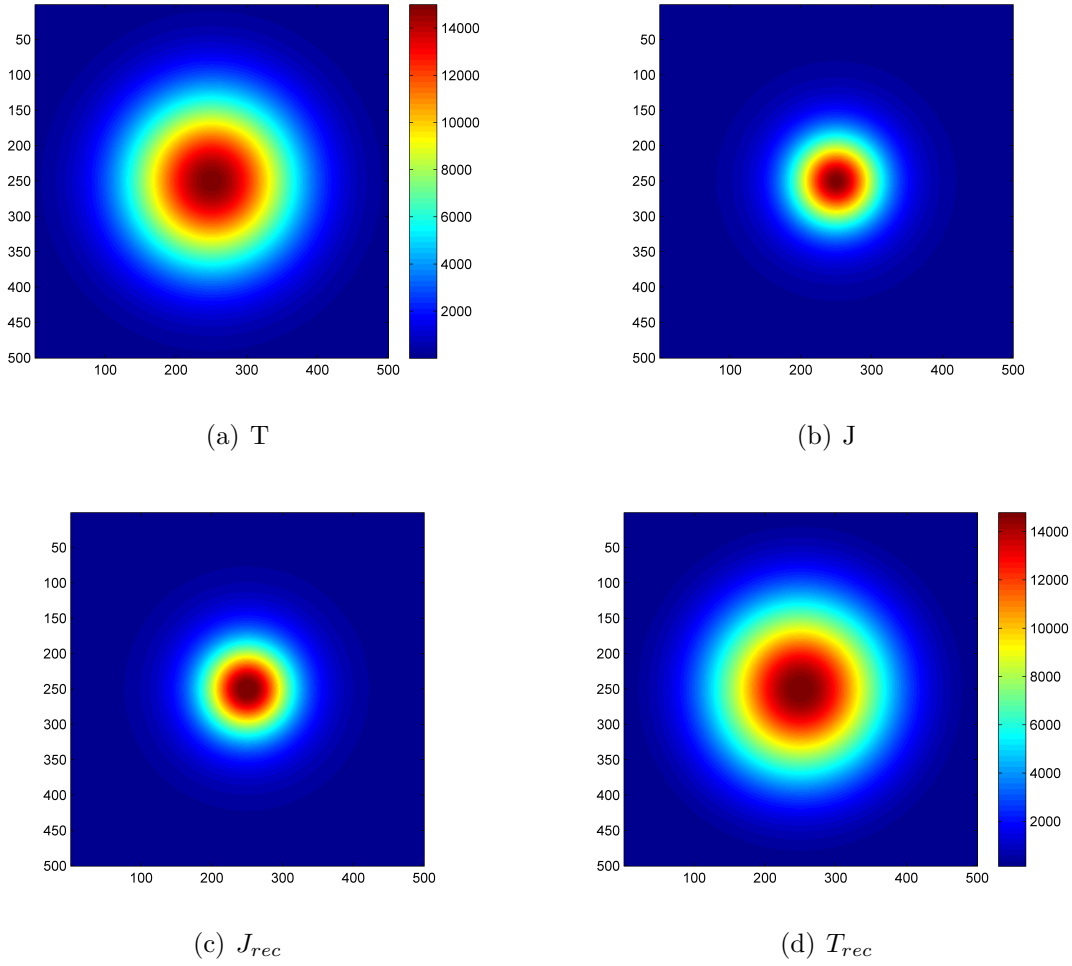


Figure 4.2: Reconstruction of a simple temperature distribution

quality of the hole placed in the middle of the distribution.

The error when measuring the temperature in the middle of the distribution (central hole) is of the order of the 30%, which is significant. In any case, any other measurement away from the central hole will give errors of the order of 1 - 2%, meaning that when reconstructing hollow distributions, the values obtained are valid everywhere except on the central hole.

The last case studied corresponds to a stretched distribution. For this case, noise is entered, in order to increase the difficulty of the recreation. For such a distribution the result is not really good in terms of shape comparison, but the RMSE is still low, and the error of the central temperature is just 6%.

Regarding the low error values obtained with the tomography, which is understood as the most accurate and reliable method, it might be possible to do a strong approximation in order to have a fast estimation of the temperature and keeping low error values. This approximation consists on assuming that there is an homogeneous and isothermal column of gas, instead of a distribution. The results obtained will be compared by means of the central temperature with

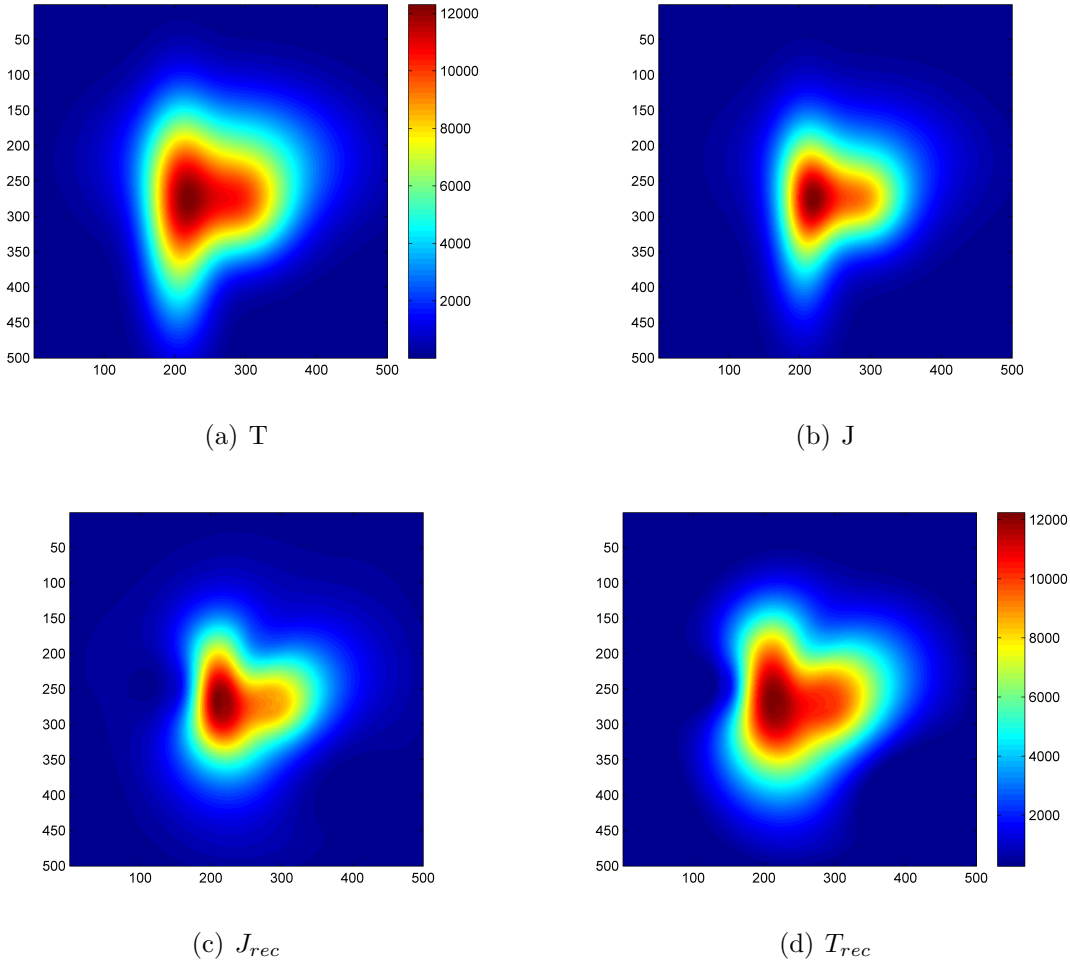


Figure 4.3: Reconstruction of an irregular temperature distribution

those of the initial and the tomography-reconstructed values.

$$I_0 = \int J(x, \frac{y_{max}}{2}) dx \quad (4.3)$$

Equation 4.3 gives the intensity at point 0, which corresponds to a line going through the center of the distribution. The integral can be done along any direction that passes through the center.

As for operating with Matlab the local emission is discretized, equation 4.3 can also be written as:

$$I_0 = \sum_{x=1}^{x_{max}} J(\cdot, \frac{y_{max}}{2}) \quad (4.4)$$

As the emission is assumed to be constant along the distance l , which is the reasonable distance along which the distribution is greater than a 20-30% of its maximum, equation 4.3 can be written as:

$$I_0 = J'l \quad (4.5)$$

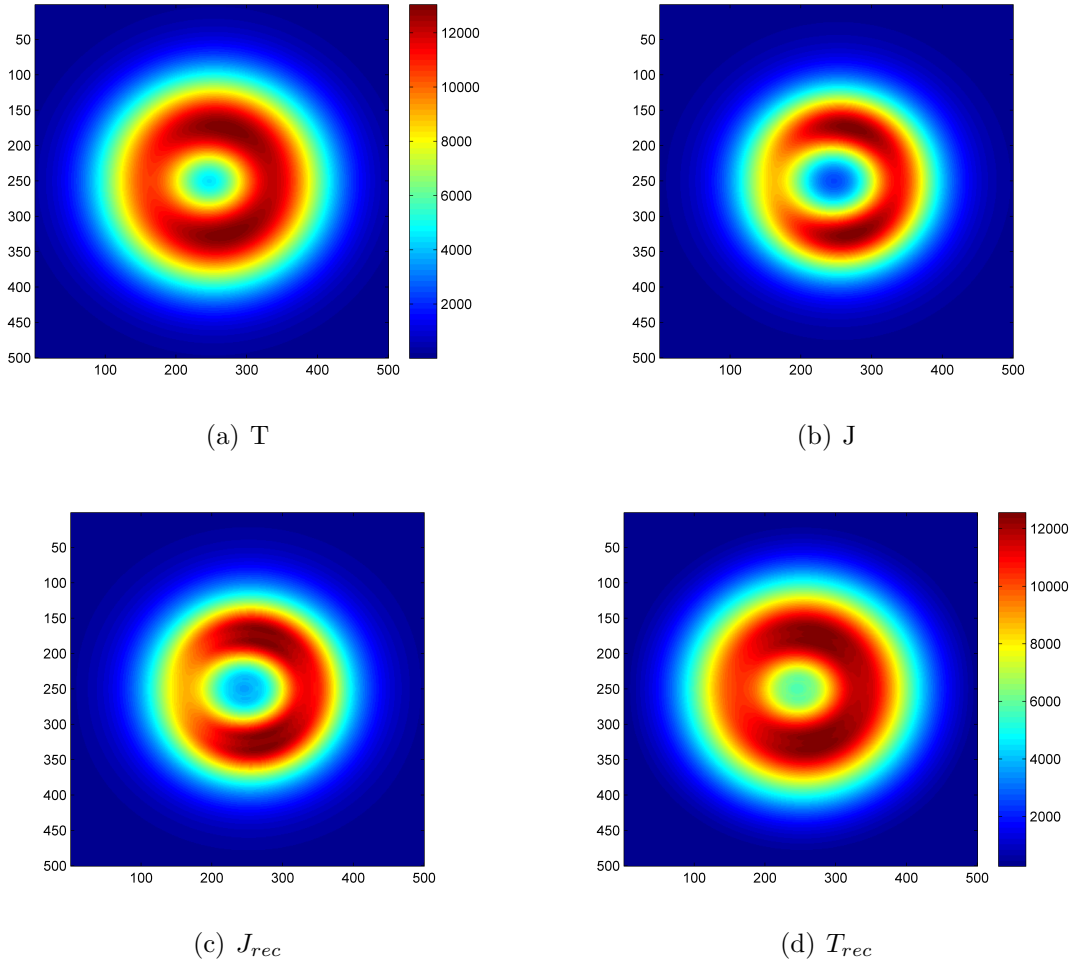


Figure 4.4: Reconstruction of a hollow temperature distribution

That can be rewritten as $J' = I/l$. This way, it is created a isothermal distribution (J') occupying the same effective area as the real distribution. With that value of J' , the temperature can be computed thanks to the relations established before.

Doing all this process for the simple, reference distribution, a temperature of $14145K$ results from this approximation method. Taking into account that the initial maximum value was $15000K$, it can be concluded that this rapid method of computing the maximum temperature is reliable, as an error of about the 5% is obtained. In any case, this simple distribution case is a good scenario for making such a big assumption. In the following table, some values computed similarly for the hollow, irregular and stretched distributions are shown:

4.2 Application to a Xenon Plasma Jet

Typical Electric ionic Propulsion systems work with Xenon. This gas is preferred among others like mercury or argon as it is not hazardous and its great mass compared with other inert gases provides greater thrust for the same power input, among other features [4].

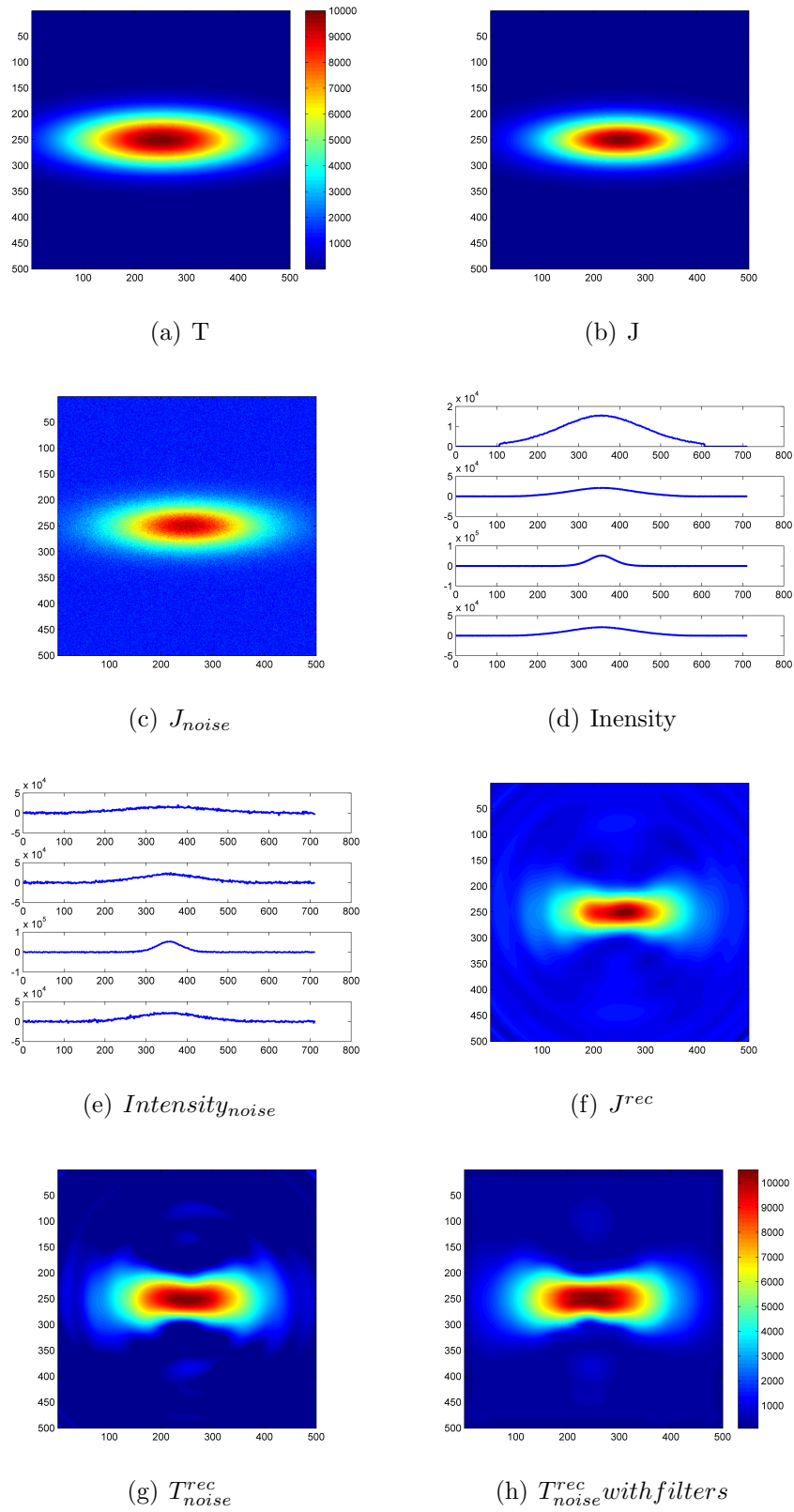


Figure 4.5: Reconstruction of a stretched temperature distribution

	<i>simple</i>	<i>hollow</i>	<i>irregular</i>	<i>stretched</i>
$T_{initial}$	15000	12000	12000	10000
$T_{central}^{rec}$	14760(1.4%)	8680(27.6%)	11880(1%)	9320(6.8%)
$T_{isothermal}$	14145(5.7%)	8740(27.2%)	10220(14.8%)	5180(48.2%)

Table 4.2: Comparison of values obtained; temperatures in Kelvin and errors shown in parenthesis

The computations of the temperature done in the previous section are just one way of computing it, when just one emission distribution is available. Here another more complex case arises; the emission has been related just with the temperature, but in fact, this property is proportional also to the number of emitting species (that could be atomic or molecular, in this case they are atomic) present. The greater the number of particles, the greter the local emission.

Thus, it might be interesting to determine both the temperature and the density distributions. But as this way there are two unknowns, two equations will be needed. The relation between the local emission J and the density N and temperature T is given by equations 4.6 and 4.7.

$$J_i(x, y) = N_i A_i h c \sigma_i \quad (4.6)$$

$$N_i(x, y) = N_{tot}(x, y) \exp \frac{-E_i}{T(x, y)} \quad (4.7)$$

The subindex i indicates all the terms that are related to the emission and that will change up to it. With this equation estated, it will be necessary to find out two different emission distributions $i = 1, 2$ in order to have a compatible determined system of equations. The way the emission was defined before, it seems impossible to distinguish between two different emission distributions. But in fact, it is not difficult to do it.

In order to explain the process it is needed to move to the atomic charachter of the flow. The light that can be seen is just energy lost by the atoms composing the flow. These atoms have electrons excited. By excited it means that the electrons are located in high energy layers, far away from the ground state (the layer close to the core). The light emission observed comes from the energy released by the electrons jumping from high energy layers to low energy layers (see Figure 4.6 for a didactic example). That energy released is proportional to $h c \sigma$, being h the Planck constant, c the speed of light and σ the wavenumber.

Thus, when different layers are present, all electrons jumping from different layers will provoke emission distributions at different wave legths that can be recorded separately. Then, J_1 and J_2 can be computed, and dividing one over the other, equation 4.8 is achieved.

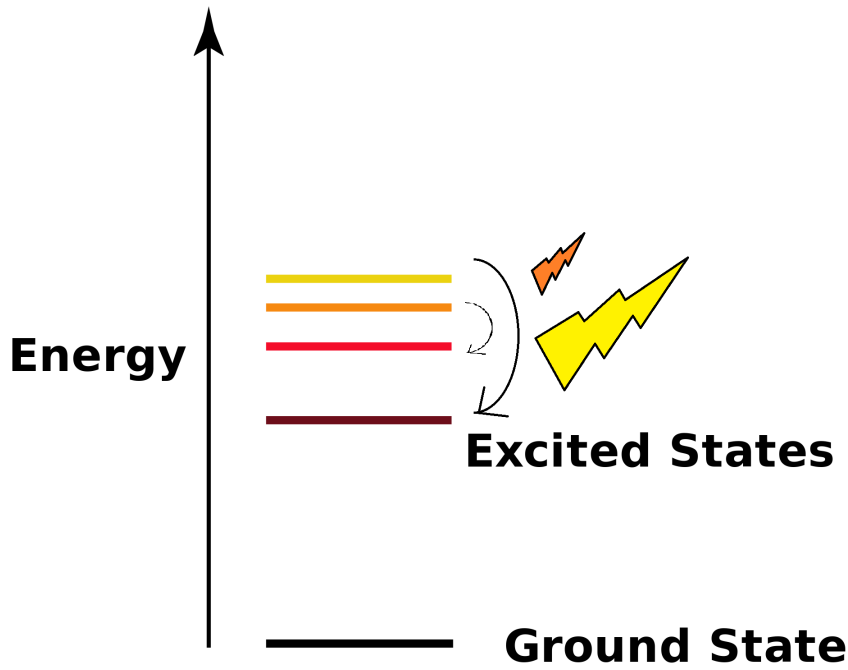


Figure 4.6: Light emitted due to electrons

$$T(x, y) = \frac{-\Delta E}{\log K} \text{ with } K = \frac{J_1 A_2 hc\sigma_2}{J_2 A_1 hc\sigma_1} \quad (4.8)$$

This equation relates the temperature with the emission quotient. Thus, now there is only one unknown and one equation, and the temperature can be computed. Then, with T , equations 4.6 and 4.7 can be used to get also the density reconstruction.

Figure 4.7 shows all images corresponding to the steps of the process. The experimental data available was the the density radial distribution. From it, assuming axial symmetry of the flow, it was reconstructed figure *a*. Then, thanks to this density distribution, it was created artificially the temperature distribution of *b*. There is only temperature on the area accupied by particles, which is determined by the density distribution. The temperature chosen was 10000 K, which is 1 eV¹, the minimum energy needed to emit light. With formulas 4.6 and 4.7, emission distributions *c* and *d* were created.

At this point, the tomography method was implemented, in order to get $J_{1,2}^{rec}$. Those are not shown as the tomographic technique has been already proven. What is shown in *e* is the quotient J_1^{rec}/J_2^{rec} . This is an important factor, as it is a typical source of undetermined solutions. In the figure it is shown a random line crossing the center. It can be seen a constant value altered by some peaks. Those peaks come from dividing great numbers over small ones

¹electron volt

or vice versa. In fact, if we were doing this to the original emission reconstructions, we would get ∞ and *NaNs* as solutions. Due to this behaviour, the temperature distribution resulting will only be reliable in the central zone where stable behaviour rule. In step *f* it is seen that in that central zone the result coincides totally with the initial one of 10000 K (dark blue). Away from it, a truncation had to be applied in order to get rid of the bad results coming from the emission quotient.

Finally, the density is reconstructed using this temperature distribution and one of the emission distributions. Surprisingly, even though the temperature was filtered before reconstructed, the density reconstruction matches completely the initial one.

Thus, it has been shown how a good density and temperature distributions can be reconstructed starting with just two emission distributions.

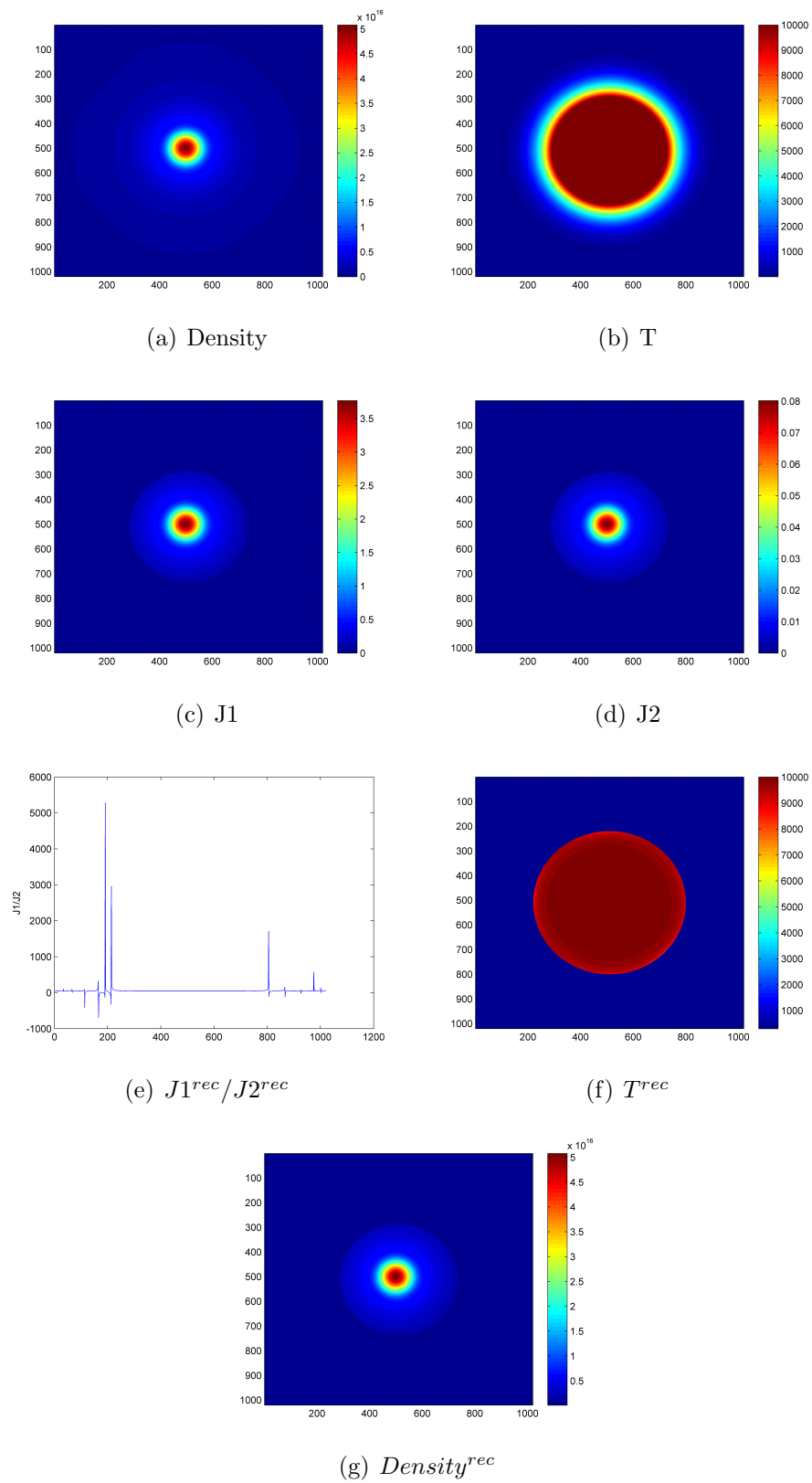


Figure 4.7: Reconstruction of the temperature and the density distributions

Chapter 5

Summary & Conclusions

During this report it has been shown an alternative method of obtaining distributions of different properties of a reactive flow. Recall the initial objectives, which included:

- Achieving a functional program able of making emission reconstructions.
- Critical analysis of its functionality, determining its limitations.
- Implementing the code in a realistic environment in order to check its performance when dealing with realistic data.

All the objectives have been covered, although the last one could have been covered in a greater extent if real experiments could have been done. Sadly, this was not viable and already-taken measurements had to serve to our purpose.

The principal conclusion extracted from the whole development of the program and further analysis is the fact that tomographic techniques are really powerful, and that they should be widely implemented. During this project, with a simple implementation of this techniques, really good results were achieved. The tomography used in more advanced disciplines (like medicine) are much more complex, so that if those technologies were applied to this field, greater projects could be done, resulting in really powerful tools.

In particular, it has been shown the different shapes that distributions should have for the code to recreate them in a realistic way. During the whole report, it has been studied a really important distribution as it is the hollow one. In experimental situations, a high percentage of real jets leave the exhaust with this shape, as it is typical of some electric propulsion systems to have annular shapes. Then, the hollow distribution will evolve to a replete. This evolution is the reason why this method is so important, as it gives the opportunity of recreating all chopped sections of a real jet, being able to track a jet at every single point of its development.

Regarding the realistic cases analysed, it was shown how temperature distributions are easily reconstructed. On the other hand, when including the density of particles as an active part of the equation, the quality of the temperature reconstruction was lowered on the edges due to

the reasons explained in section 5.2. The final density reconstruction had a really good quality, and the temperature in the central zone, the significant one, was properly reconstructed. Thus, as both unknowns were properly reconstructed, the results could be used with total confidence.

5.1 Future steps

The next step in a tactical level, once the program is working, would be to test it in a real experiment. For this purpose, a more complex software could be created in order to have easy and fast access to the reconstruction technique.

On a more strategic level, improved tomographic methods should be implemented, together with a technological advance in terms of the recording systems. Here there is an advantage with respect to medicine, it is the fact that reactive jets emit light by themselves, there is no necessity of adding an external source. Thus, with those technological advances, even greater results than in medicine could be achieved. Regarding the applicability of the technique, some other properties apart from the temperature and the density of species could be inferred out of the emission distribution. Light can be related to several properties, and its relations are totally available.

In conclusion, the applicability of the method is really high, and, together with some technological improvements, it can be used to achieve high quality characterizations of several properties of a reactive flow jet.

Appendices

Appendix A

Trigonometric Interpolation

$$c_n(\theta) = \frac{1}{2}a_{n0} + \sum_{m=1}^{K-1} (a_{nm} \cos m\theta + b_{nm} \sin m\theta) \quad (\text{A.1})$$

being:

$$a_{nm} = \frac{1}{K} \sum_{k=1}^{2K} c_n(\theta_k) \cos m\theta_k \quad (\text{A.2})$$

$$b_{nm} = \frac{1}{K} \sum_{k=1}^{2K} c_n(\theta_k) \sin m\theta_k \quad (\text{A.3})$$

Assuming that the fluid under study is optically thin, that is, the optical radiation of the medium is well attenuated, it can be established that:

$$c_n(\theta_{K+k}) = c_n(\theta_k + \pi) = (-1)^n c_n(\theta_k), k = 1, 2, \dots, K \quad (\text{A.4})$$

With this, a_{nm} and b_{nm} can be written as:

$$a_{nm} = \begin{cases} \frac{2}{K} \sum_{k=1}^K c_n(\theta_k) \cos m\theta_k & \text{if } n+m \text{ is even,} \\ 0 & \text{otherwise} \end{cases} \quad (\text{A.5})$$

$$b_{nm} = \begin{cases} \frac{2}{K} \sum_{k=1}^K c_n(\theta_k) \sin m\theta_k & \text{if } n+m \text{ is even,} \\ 0 & \text{otherwise} \end{cases} \quad (\text{A.6})$$

Appendix B

Budget

It is important to realise which value would have the project if it had been done within the industrial environment. For that reason, a sketched budget is going to be done, which would serve as orientation of the final economic value of the product.

- **Direct Investment:**

- Computer.....600€
- Engineer Hours.....15 € per hour
- Matlab License.....2000 €

- **Indirect Investment:**

- Energy Consumption.....35€
- CCD Cameras.....3200 € each
- Worker in charge.....8 € per hour
- Devaluation of the material..... 2000 € per year

The price of the computer is that on the one used actually for the development of the program. The engineer and worker salaries are plain estimations. The price of the energy was obtained through *Tarifasgasy luz* webpage, taking into account the number of hours employed for this investigation was 300 hours. This value must be applied also to the engineer hours price.

The CCD cameras price is given per unit, as it is a choice of the company the number of cameras to use. It will be used four as sample value. The unitary price established was estimated from *Sbig* company prices. For the worker in charge, who will be assumed to be in charge of the usage of the program and the maintenance, it will be estimated that he works 20 hours per year due to this specific tasks.

With this information, the total initial investment would be 19935€ (from which 7135€ correspond to the research project itself and 12800€ to the CCD cameras) plus 2160€ per year.

Bibliography

- [1] Y. Babou, F. Cannat, and D. Lequang. Tomography by means of a single ccd camera. 2013.
- [2] P. Toft. The radon transform: Theory and implementation. 1996.
- [3] J. Hlína, F. Chvála, J. Sonský, and J. Gruber. Multi-directional optical diagnostics. 2007.
- [4] D.M. Goebel and I. Katz. Fundamentals of electric propulsion. 2008.